BNL-225133-2023-JAAM

GRP-AEM-7

Magnetic ac susceptibility of superconducting Ta films for quantum computing

J. Yao, Q. Li

To be published in "Superconductor Science and Technology"

January 2024

Condensed Matter Physics and Materials Science Department

Brookhaven National Laboratory

U.S. Department of Energy

USDOE Office of Science (SC), Basic Energy Sciences (BES)

DISCLAIMER

Magnetic ac Susceptibility of Superconducting Ta Films for Quantum Computing

Juntao Yao[1, 3], Chenyu Zhou[2], Pedro Mercado Lozano[1, 4], Sarah Paone[1, 4], Mingzhao Liu[2] and Qiang Li[1,4a]

[1] Condensed Matter Physics and Materials Science Department, Brookhaven National Laboratory, Upton, USA
[2] Center for Functional Nanomaterials, Brookhaven National Laboratory, Upton, USA
[3]Department of Materials Science and Chemical Engineering, Stony Brook University, Stony Brook, USA
[4]Department of Physics and Astronomy, Stony Brook University, Stony Brook, USA

E-mail: qiangli@bnl.gov
Received xxxxxx
Accepted for publication xxxxxx
Published xxxxxx

Abstract

Recently, breakthroughs were reported in the long coherence time (> 0.5 ms) transmon qubit using tantalum films (Ta). Identifying the loss mechanism in Ta films will help further improve the performance of Ta-based superconducting qubits. Here, we report a study of superconducting properties in two sets of Ta films grown on c-cut and a-cut sapphires respectively using contact transport and noncontact magnetic ac susceptibility measurements. Although the resistive transition appears to be similar in both films, we found strikingly different responses in their complex magnetic susceptibilities $\chi' + i\chi''$. χ'' in the c-cut films exhibits a sharp peak at superconducting transition T_c and becomes featureless below T_c indicating a strongly coupled superconducting state. In contrast, χ'' in the a-cut films exhibits a broad peak near T_c and a second peak appears below T_c, indicating granular superconductivity behavior. This second peak in χ'' is associated with the hysteresis loss at weak-link-type grain boundaries, which is believed to be a leading source of decoherence in the a-cut Ta films. The derived magnetic loss tangent in the a-cut films is about one order of magnitude higher than in the c-cut films. This study demonstrates that ac susceptibility is an excellent probe for characterizing bulk superconducting properties of the constituent superconducting materials used in qubits.

Keywords: quantum computing, superconducting qubits, loss tangent, ac susceptibility, superconducting Ta films

1. Introduction

In recent years, quantum information has become an area of the technology race worldwide. At the forefront is the development of low-loss, long-coherence, or fault-tolerant quantum computation technologies. Among them, Josephson junctions underlying the operations of superconducting qubits [1, 2] stand out as a key enabler for quantum computers. In 2019, "Quantum Supremacy" was claimed by Google using a processor with 54 programmable superconducting qubits [3]. Then, in 2021, IBM built its Eagle quantum computer with 127 superconducting qubits [4]. While these developments are exciting, there remains significant work ahead in superconducting qubits to reduce the decoherence effect, a crucial performance limiting factor in quantum computers [5, 6].

Among primary causes of decoherence in superconducting qubits are charge noise, critical current noise, dielectric loss, flux noise, etc. [7-9]. Over the last two decades or so, many efforts have been made to improve the coherence time from a nanosecond in a Cooper pair box by Nakamura et al in 1999 [10] to hundreds of nanoseconds in a modified charge qubit

(the quantronium qubit) by Vion et al. in 2002 [11]. A persistent current flux qubit brought coherence times into a few microsecond range [12]. The "transmon" qubit developed by Schoelkopf and co-workers significantly reduced the charge sensitivity of the Cooper pair box [13, 14]. That development has led to the increase of T_2 above 20 μs with a persistent-current flux qubit in a 2D geometry using dynamical decoupling sequences [15]. The T_2 coherence time had been further increased to ~100 μs [16] by using a 3D-cavity approach developed at Yale University [17]. In 2020, a Princeton University group reported Ta film based transmon qubits that increased the coherence time to 300 μs [18]. Soon after, Wang et al. obtained transmon qubits with the best T_1 lifetime of 503 μs in 2021 [19]. This achievement was made possible by replacing traditional Nb with Ta as the base superconductors used in the qubit devices. While Ta-films brought the record high coherence time in recent developments, our knowledge on the structural and property relationship in superconducting Ta films is very limited. This knowledge is crucial for identifying the origin of decoherence and further improvement of the Ta-based qubits, and this is the primary motivation for the work we report here. The second motivation of our study is the need to develop more noncontact techniques for characterizing superconducting films and qubits, such as the magnetic ac susceptibility method we report here.

Contact electrical resistance measurements are the conventional method used to characterize the bulk properties of constituent qubit materials through the determination of superconducting transition temperature T_c and the Residual Resistance Ratio (RRR) value. In this study, we performed both contact resistivity and noncontact dc and ac magnetic susceptibility measurements of two sets of superconducting Ta films grown on a- and c-cut sapphire substrates. We report remarkably different characteristics of ac susceptibility in spite of the similarity of their resistance and dc susceptibility. The resulting ac susceptibility was used for calculating magnetic loss tangent which may be used to evaluate the coherent properties of Ta-based superconducting qubits.

2. Methods

2.1 Thin Film Growth

Ta films were grown on two-inch sapphire substrate wafers purchased from CrysTec. Both a-cut and c-cut wafers are single-side polished. Ta thin films are deposited by magnetron sputtering (AJA Orion) at 750°C. The Ta sputtering target was purchased from AJA International, having a purity of 99.98%. The target dimensions stand at 1.5 inches in diameter and 0.188 inches in thickness. Before being loaded into the deposition chamber, the sapphire wafers undergo a cleaning process involving the use of a piranha solution. This solution

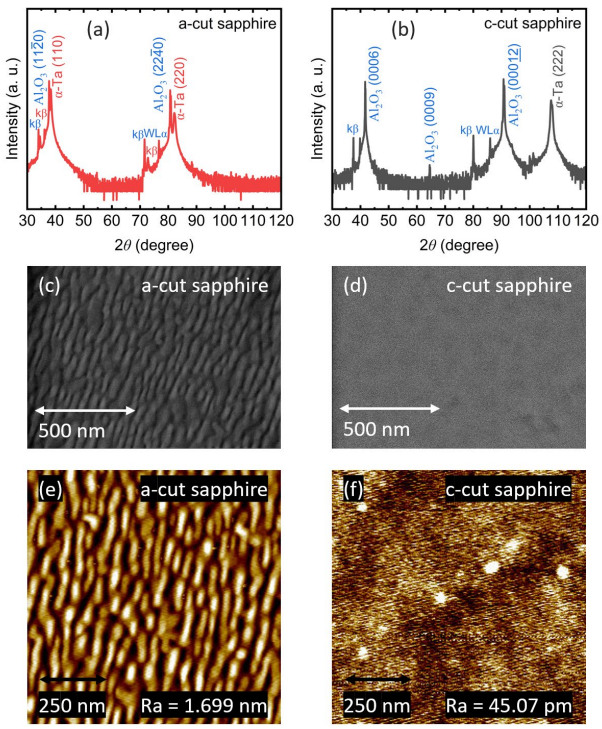

Figure 1. (a) and (b): XRD patterns confirm both Ta films grown on a- and c-cut sapphire are *bcc* α-phase; the surface morphology studied by SEM and AFM of Ta thin films grown on a-cut sapphire: (c) and (e), grown on c-cut sapphire: (d) and (f). Both SEM and AFM images show elongated grain structure on the a-cut Ta film, while no visible features on the c-cut Ta film. Note that the sparkling dots seen in (f) are environmental dust.

is prepared by combining 30% hydrogen peroxide solution and 98% sulfuric acid in a volume ratio of 1:2. Subsequently, the wafers are thoroughly rinsed with deionized (DI) water. Following the evacuation of the chamber to 10^{-6} Pa, argon (Ar) was introduced to sustain a stable working pressure of 1 Pa. The sputtering power was 100 W and the sputtering rate was controlled at 3 nm/min. The thickness of the grown Ta films is about 120 nm, which is chosen to be comparable to the typical Ta film thickness used in actual qubit devices [18, 19]. The Ta thin films were characterized using X-ray diffraction (XRD) on a Rigaku SmartLab II diffractometer, employing Cu Kα radiation with a wavelength of 1.5418 Å. XRD patterns indicate both Ta films grown on a-cut and c-cut sapphire substrate were pure *bcc* α-phase as shown in Fig. 1 (a) and (b). The Scanning Electron Microscope (SEM) images (scan size 10 μm × 10 μm) and Atomic Force Microscopy (AFM) images (scan size 1 μm × 1 μm), shown in Fig. 1 (c) – (f), were taken with Hitachi S-4800 Scanning Electron Microscope and Park AFM, showing the surface morphology of Ta thin films grown on a- and c-cut sapphire substrates. Images from both SEM and AFM are highly consistent, showing that the Ta thin films grown on the a-cut sapphire substrates (Fig. 1 (c) and (e))

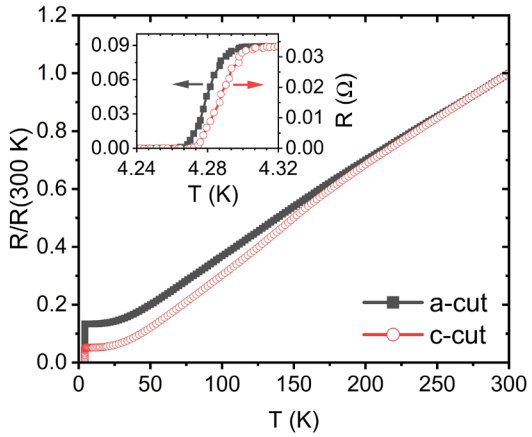

Figure 2. Normalized electrical resistance vs temperature for Ta films grown on a-cut (black) and c-cut (red) sapphire substrates; the critical temperatures T_c are 4.28 and 4.30 K, respectively. (Inset) The non-normalized resistance vs temperature for both films, in the unit of ohm, within the range near the T_c.

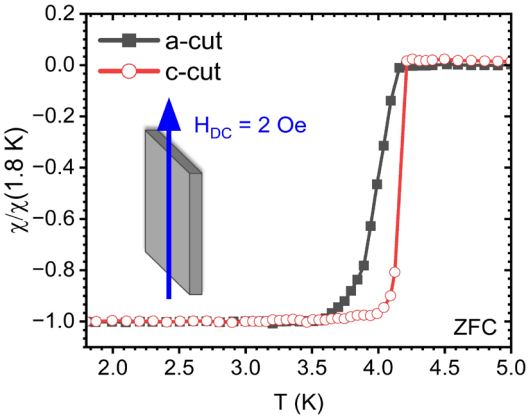

Figure 3. Zero-field cooling DC magnetic susceptibility for Ta films grown on the a-cut (black) and c-cut (red) sapphire substrates. A 2 Oe field is applied along the films' surface. The susceptibility is normalized at temperatures T = 1.8 K.

display a distinct elongated granular structure. In contrast, the Ta thin films on the c-cut sapphire substrates (Fig. 1 (d) and (f)) are very smooth with no visible features at the equivalent magnifications. The Root Mean Square (RMS) roughness value (R_a) measured by AFM is 1.699 nm for the a-cut films and 45.07 pm for the c-cut films.

2.2 Transport and Magnetic Susceptibility Measurement

Transport measurements were carried out utilizing the standard four-probe inline method on the film surface in a 14 Tesla Quantum Design physical properties measurement system (PPMS). A 50 μA alternating current was applied to each sample using gold (Au) electrical contact wires. For examining the magnetic properties, both dc and ac magnetic susceptibility were measured in a Quantum Design magnetic properties measurement system (MPMS) with a SQUID (superconducting quantum interference device) magnetometer in the temperature range of 1.8 - 5 K. The applied magnetic field for the dc susceptibility measurement was 2 Oe and parallel to the films' surface. The ac susceptibility measurements were conducted under a zero dc field, with applied ac drive amplitudes of 1 Oe and 5 Oe applied parallel to the films's surface at a frequency of 1500 Hz.

3. Results and Discussion

Fig. 2 shows the measured electrical resistance plotted as a function of temperature for two sets of Ta films. In both cases, the resistance is normalized to the value at temperature T = 300 K. The inset is the non-normalized resistance within the range near the T_c (4.24 - 4.32 K). Both the a- and c-cut films exhibit a sharp superconducting transition at the critical temperature of 4.28 and 4.30 K, respectively. The Residual Resistance Ratio (RRR) values have been calculated to be 7.48 for the a-cut film and a significantly higher value of 19.36 for the c-cut film. This difference in RRR values indicates the higher quality of the c-cut film.

Fig. 3 presents the data of zero-field cooling (ZFC) dc magnetic susceptibility $\chi(T)$ versus temperature in a temperature range of 1.8 K to 5.0 K with an applied external field of 2 Oe parallel to the film surface. The measured data was normalized by the magnetic susceptibility at temperature T = 1.8 K. The onset superconducting transition temperatures T_c^{onset} are 4.18 K and 4.21 K for the a- and c-cut Ta films, respectively. These temperatures are slightly lower than the values determined from resistance measurements. As temperature decreases below T_c^{onset}, the a-cut film demonstrates a mildly broad transition in susceptibility.

It has been known that ac magnetic susceptibility measurements can provide valuable information on the superconducting grain connectivity since the earlier days of investigating the grain coupling behaviour in polycrystalline high-T_c cuprate superconductors [20, 21]. In a granular superconductor, the critical temperature T_c is determined from the real part of the ac susceptibility, while the features of the imaginary component are used to characterize the energy loss arising from the weak inter-grains coupling.

In granular superconductors, the grain becomes superconducting at T_c first, then the entire sample becomes superconducting at a lower temperature once Josephson coupling is established across grain boundaries. This leads to a step in the real part of magnetic susceptibility, χ', and a

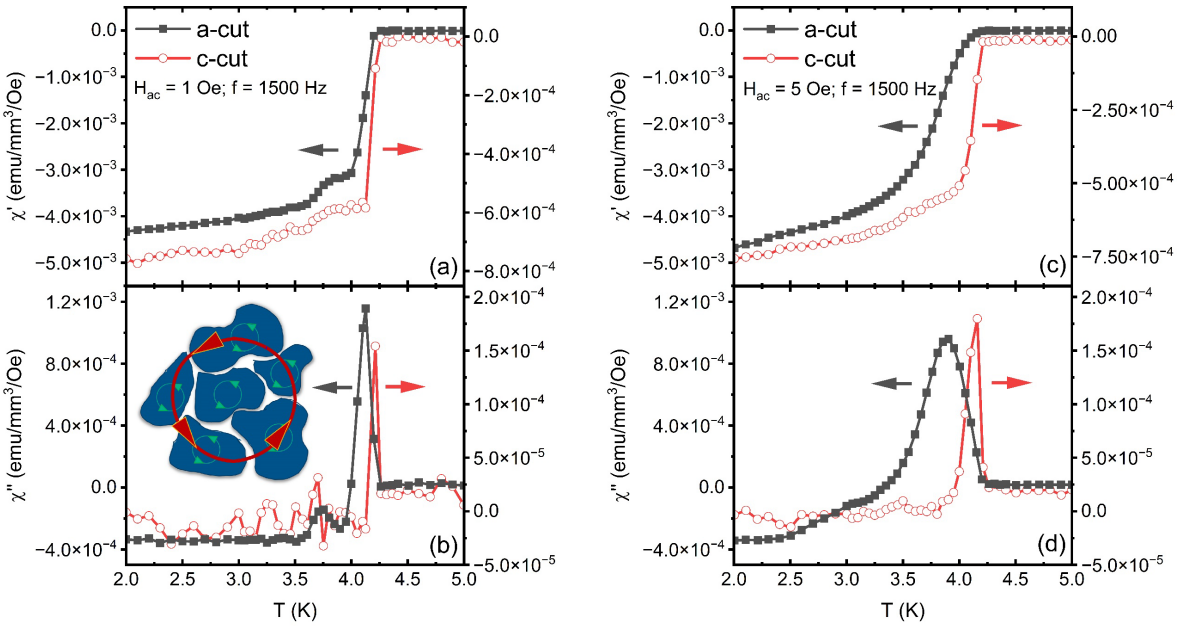

Figure 4. AC magnetic susceptibility of Ta films grown on a- (black lines) and c-cut (red lines) sapphire substrates, measured under a drive amplitude of 1 Oe in panels (a) and (b), and 5 Oe in panels (c) and (d). The upper panels display real parts, and the lower panels are imaginary parts. A second transition and a peak are obvious at 3.80 K for the a-cut film under a 1 Oe measurement. As the drive amplitude increases to 5 Oe, this second transition in the real part merges with the intrinsic superconducting transition, while the second peak in the imaginary part broadens and shifts to a lower temperature. The inset to (b) is a sketch showing the intra (green circles)- and inter (a red circle)-screening currents in a granular superconductor.

second peak in the imaginary part, χ''. This is precisely what we observed in the Ta films on the a-cut substrates, but *not* on the c-cut substrates, as demonstrated in Fig. 4, where the real and imaginary components of the ac susceptibility, $\chi'(T)$ and $\chi''(T)$ are plotted as a function of temperature. A sketch of the intra- and inter-screening currents is shown in the inset of Fig. 4. In the inset, the separation between grains is exaggerated to emphasize the Josephson coupling behavior in the granular superconductors. In actual samples, like our Ta-films, grains are well connected without a gap. When the temperature is lowered to reach the critical temperature T_c, the individual grains within the sample become superconducting, thus screening out external magnetic field by the intra-grain supercurrent (denoted by the small green circle). As the temperature continues to decrease, Josephson coupling between the grains increases, eventually driving the entire sample into a superconducting state. The magnetic field is screened out of the entire sample by inter-grain supercurrent (denoted by the big red circle in the inset of Fig. 4) [22].

As illustrated in Fig. 4a and 4b, under an applied drive amplitude as low as 1 Oe, the onset critical temperatures T_c^{onset} in the real part $\chi'(T)$ are 4.20 and 4.26 K, with the peak positions in the imaginary part $\chi''(T)$ at 4.13 and 4.21 K for the a- and c-cut films, respectively. Note: for direct comparisons, different y-axis scales are used to plot the ac susceptibility as a function of temperature in Fig. 4. Our SQUID ac susceptibility has a sensitivity of the order of a few 10^{-5} emu/mm^3/Oe, which is reflected by the noise level of the χ'' of the c-cut films (the right y-axis) in Fig. 4(b). For all these films, the onset temperature and peak location are generally consistent with the results from our resistance and dc susceptibility measurements. The $\chi'(T)$ curve for the a-cut film shows a somewhat broader transition compared to that of the c-cut film and also a second transition at 3.80 K. In $\chi''(T)$, a distinct second peak is clearly observed at 3.73 K. This second peak corresponds to the second transition in $\chi'(T)$, suggesting the weak coupling of the grains in the a-cut film sample.

Upon increasing the drive amplitude to 5 Oe, the T_c^{onset} in the real part of the susceptibility for the a- and c-cut films shift to 4.10 and 4.21 K. Concurrently, the second transition previously noted at 3.80 K in the a-cut film merged with its first peak in the higher temperature. A larger field driven shift of the broader imaginary peak position to a lower temperature (4.10 K to 3.88 K) is observed for the a-cut films, while the (4.21 K to 4.12 K) shift is modest in the c-cut films with a very little broadening in $\chi'(T)$ and $\chi''(T)$. In comparison, no second peak in $\chi''(T)$ was observed for the c-cut films in high field. The slight broadening of $\chi'(T)$ and $\chi''(T)$ near T_c in the c-cut films at high fields is a generic feature of field

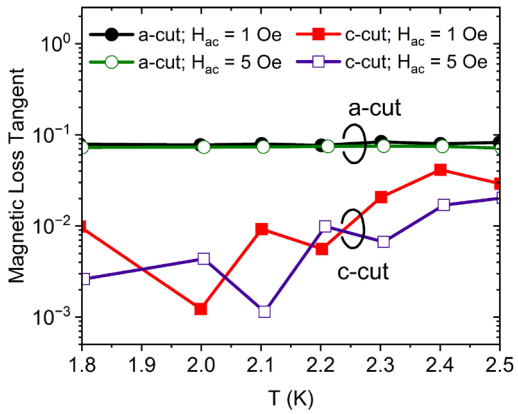

Figure 5. The calculated magnetic loss tangent for a- and c-cut Ta films at two applied magnetic fields.

suppressed superconducting transition temperature $T_c(H)$, which is known to increase the superconducting transition width in the temperature dependent resistivity and magnetization.

From the ac magnetic susceptibility measurement, we calculated the magnetic loss tangent using the following expression:

$$\tan(\delta) = \left|\frac{\chi''(T)}{\chi'(T)}\right| \quad (1)$$

Fig. 5 shows that the calculated magnetic loss tangent in the a-cut films is approximately one order of magnitude higher than that in the c-cut films. This is observed in both 1 Oe and 5 Oe drive amplitude measurements within the low-temperature range. It appears that the difference in the loss tangent of these two sets of films increases when temperature decreases, which suggests the c-cut films will have even better performance than that of the a-cut films at qubit operating temperatures below 100 mK.

4. Conclusions

In this study we reported superconducting properties, in particular, the grain connectivity in Ta thin films grown on a- and c-cut sapphire substrates using non-contact ac magnetic susceptibility measurements. We found that while critical temperatures characterized by the common methods of electrical resistance and dc magnetic susceptibility measurements are similar, their complex ac magnetic susceptibilities are significantly different. The Ta films grown on the c-cut sapphire substrates display a sharp superconducting transition in both the real part $\chi'(T)$ and imaginary part $\chi''(T)$, indicating a strongly coupled superconducting state. In contrast, the a-cut Ta film displays granular superconductivity behaviour characterized by a broad transition and double peaks appearing near the superconducting transition in $\chi'(T)$ and $\chi''(T)$, respectively. These features are consistent with the behavior of a granular superconductor with weak grain boundary coupling.

Through our ac magnetic susceptibility measurements, the magnetic loss tangent in the a-cut films is found to be roughly an order of magnitude higher than that in the c-cut films, presumably related to elongated grains in the a-cut films. We note that the Ta films having reported high decoherence times of 0.3 ms for qubit devices were grown on the c-cut sapphire substrates [18]. The other question is whether the a-cut Ta-films are more likely to form surface oxide which can lead to higher dielectric loss and thus decrease qubit coherence time. Clearly, further studies are needed to clarify the detailed structure-property relationship in Ta films, as well as the growth-property relationship. The ultimate goal is to identify and understand the causes of decoherence in Ta films that are critical to the improvement of the performance of Ta-based superconducting qubits in quantum information applications. The ac magnetic susceptibility measurement we demonstrated in this study is a useful tool for the evaluation of dissipative loss of superconducting materials used in qubits, thus a step to achieve this goal.

5. Acknowledgments

JY, PML, SP, and QL are supported by the US Department of Energy, Office of Basic Energy Science, Materials Sciences and Engineering Division, under contract number DE-SC00112704. CZ and ML are supported by the U.S. Department of Energy, Office of Science, National Quantum Information Science Research Centers, Co-design Center for Quantum Advantage (C2QA), under Contract No. DE-SC0012704. This research used the Materials Synthesis and Characterization facilities of the Center for Functional Nanomaterials (CFN), U.S. Department of Energy Office of Science Facilities at Brookhaven National Laboratory, under Contract No. DE-SC0012704

6. References

[1] Makhlin Y, Schön G and Shnirman A 2001 Quantum-state engineering with Josephson-junction devices *Rev. Mod. Phys.* **73** 357

[2] Clarke J and Wilhelm F K 2008 Superconducting quantum bits *Nature* **453** 1031

[3] Arute F et al. 2019 Quantum supremacy using a programmable superconducting processor *Nature* **574** 505

[4] Bhat H A, Khanday F A, Kaushik B A, Bashir F and Shah K A 2022 Quantum Computing: Fundamentals, Implementations and Applications *IEEE Open J. Nanotechnol.* **3** 61

[5] Van Harlingen D J, Robertson T L, Plourde B L T, Reichardt P A, Crane T A and Clarke J 2004 Decoherence in Josephson-junction qubits due to critical-current fluctuations *Phys. Rev. B* **70** 064517

[6] Ansari M H and Wilhelm F K 2011 Noise and micro-resonance of critical current in Josephson junction induced by Kondo trap states *Phys. Rev. B* **84** 235102
[7] McDermott R 2009 Materials Origins of Decoherence in Superconducting Qubits, *IEEE Trans. Appl. Supercond.* **19** 2
[8] Oliver W D and Welander P B 2013 Materials in superconducting quantum bits *MRS Bull.* **38** 816
[9] Zeng L I, Nik S, Greibe T, Krantz P, C. Wilson C M, Delsing P and Olsson E 2015 Direct observation of the thickness distribution of ultra-thin AlOxbarriers in Al/AlOx/Al Josephson junctions *J. Phys. D Appl. Phys.* **48** 395308
[10] Nakamura Y, Pashkin Y A, and Tsai J S 1999 Coherent control of macroscopic quantum states in a single-Cooper-pair box *Nature* **398** 786
[11] Vion D, Aassime A, Cottet A, Joyez P, Pothier H, Urbina C, Esteve D and Devoret M H 2002 Manipulating the Quantum State of an Electrical Circuit *Science* **296** 886
[12] Bertet P, Chiorescu I, Burkard G, Semba K, Harmans C J P M, DiVincenzo D P and Mooij J E 2005 Dephasing of a Superconducting Qubit Induced by Photon Noise *Phys. Rev. Lett.* **95** 257002
[13] Koch J, Yu T M, Gambetta J, Houck A A, Schuster D I, Majer J, Blais A, Devoret M H, Girvin S M, Schoelkopf R J 2007 Charge-insensitive qubit design derived from the Cooper pair box *Phys. Rev. A* **76** 042319
[14] Houck A A, Schreier J A, Johnson B R, Chow J M, Koch J, Gambetta J M, Schuster D I, Frunzio L, Devoret M H, Girvin S M, Schoelkopf R J 2008 Controlling the Spontaneous Emission of a Superconducting Transmon Qubit *Phys. Rev. Lett.* **101** 080502
[15] Bylander J, Gustavsson S, Yan F, Yoshihara F, Harrabi K, Fitch G, Cory D G, Nakamura Y, Oliver W 2011 Noise spectroscopy through dynamical decoupling with a superconducting flux qubit *Nature Physics* **7** 565
[16] Rigetti C, Gambetta J M, Poletto S, Plourde B L T, Chow J M, Corcoles A D, Smolin J A, Merkel S T, Rozen J R, Keefe G A, Rothwell M B, Ketchen M B, Steffen M 2012 Superconducting qubit in a waveguide cavity with a coherence time approaching 0.1 ms *Phys. Rev. B* **86** 100506
[17] Paik H, Schuster D I, Bishop L S, Kichmair G, Catekani G, Sears A P, Johnson B R, Reagor M J, Frunzio L, Glazman L I, Girvin S M, Devoret M H, Schoelkopf R J 2011 Observation of High Coherence in Josephson Junction Qubits Measured in a Three-Dimensional Circuit QED Architecture *Phys. Rev. Lett.* **107** 240501
[18] Place A P M, Rodgers L V H, Mundada P, Smitham B M, Fitzpatrick M, Leng Z Q, Premkumar A, Bryon J, Vrajitoarea A, Sussman S, Cheng G M, Madhaven T, Babla H K, Le X H, Gang Y Q, Jack B, Gyenis A, Yao N, Cava R J, Leon N P, Houck A A 2021 New material platform for superconducting transmon qubits with coherence times exceeding 0.3 milliseconds *Nat. Commun.* **12** 1779
[19] Wang C, Li X G, Xu H K, Li Z Y, Wang J H, Yang Z, Mi Z Y, Liang X H, Su T, Yang C H, Wang W Y, Li Y C, Chen M, Li C Y, Linghu K H, Han J X, Zhang Y S, Feng Y L, Song Y, Ma T, Zhang J N, Wang R X, Zhao P, Liu W Y, Xue G M, Jin Y R, Yu H F 2022 Towards practical quantum computers: transmon qubit with a lifetime approaching 0.5 milliseconds *npj Quantum Inf.* **8** 3
[20] N Martin 1995 Superconductivity: A guide to alternating current susceptibility measurements and alternating current susceptometer design *American Journal of Physics* **63** 57
[21] Gomory F 1997 Characterization of high-temperature superconductors by AC susceptibility measurements *Supercond. Sci. Technol.* **10** 523
[22] Goldfarb R B, Clark A F, Braginski A I, Panson A J 1987 Evidence for two superconducting components in oxygen-annealed single-phase YBaCuO *Cryogenics* **27** 9